In: Photonic Crystals
Editor: Barbara Goodwin
ISBN: 978-1-63485-925-7

Chapter 2

BAND STRUCTURE OF METAL/DIELECTRIC PHOTONIC CRYSTALS

Yi-Xin Zong and Jian-Bai Xia*
SKLSM, Institute of Semiconductors, Chinese Academy of Sciences,
Beijing, P. R. China

Abstract

Owing to the photonic band gap effect, light propagation can be controlled in photonic crystals (PCs). In this way, the propagation of light can be controlled, which enables fabrication of novel photonic devices and improves properties of existing ones. The PCs containing metallic medium have attracted special interests due to the frequency-dependent of dielectric constant. Based on the numerical results of photonic band structures, many properties and applications can be predicted. Therefore, it is of both intrinsic and practical interest to develop a numerical framework capable of describing and distinguishing the photonic band structures of metal/dielectric (M/D) PCs.

The traditional plane wave expansion method is a straightforward method for numerical calculations of dielectric PCs band structures. However, for the M/D PCs, the resulting secular equation is nonlinear and hard to solve as the frequency-dependent dielectric constants are involved. In this chapter, an improved plane wave expansion method is proposed for the calculation of photonic bands of M/D PCs with the Drude dielectric

*E-mail address: xiajb@semi.ac.cn

function model without solving a nonlinear secular equation. The proposed method is applicable to all dimensional M/D PCs. For the purpose of illustration, this method was applied to the band structure calculations of one-dimensional (1D) and three kinds of two-dimensional (2D) M/D PC structures. In addition the photon density of state (DOS) is calculated along with the band structure.

PACS: 42.70Qs, 02.60Cb, 78.66Bz, 41.20Jb, 02.60Lj

Keywords: photonic crystal, metallic medium, plane wave expansion, band structure

AMS Subject Classification: 53D, 37C, 65P

Introduction

Since Yablonovitch E [1] and John S [2] first proposed the photonic band gap structures for achieving a complete control of the spontaneous emission, the PCs have aroused great interest in the optical field and developed rapidly [3–9]. PCs are periodic materials with spatial variations of dielectric constant on the order of an optical wavelength, which can control radiation field and light propagation characteristics [10].

Owing to the periodic structure, the electromagnetic (EM) modes in PCs have special features when compared to homogeneous material, such as the photonic band gap. Due to the property of acting as 'optical insulator', photonic band gap structures offer the opportunity of achieving a complete optical confinement, and a lot of novel PC-based devices have been developed [11–14]. Another interesting feature of PCs is the possibility of achieving very small group velocities associated with the flat band [15, 16]. Moreover, the DOS can engineer the atomic spontaneous emission and exhibit band gap or pseudogap structure, which is in accordance with the band structure [17–19].

There exist two types of EM modes in PCs, transverse electric (TE) and transverse magnetic (TM) modes, for which the electric and magnetic field are parallel to the interface plane respectively [20]. Unlike the dielectric/dielectric (D/D) PC, the metallic medium's dielectric function is frequency dependent and we will use the Drude model to describe it [21, 22]. In this model the dielectric function is $\varepsilon(\omega) = \varepsilon_\infty - \left(\omega_{\mathrm{p}}^2/\omega^2\right)$, where ε_∞ is the high-frequency dielectric constant and ω_{p} is the plasmon frequency [22, 23]. For the sake of simplicity, the imaginary part in the dielectric function of metal is omitted.

One of the basic problems for the PCs is the numerical calculation of the photonic band structure and the EM modes propagation. Up to now, as we know, there have been many successful calculation methods for the photonic bands of D/D PCs, but the method to calculate the band structures and EM field distribution of the M/D structures is rare [24–28]. Sakoda $et\ al.$ [25] calculated the dispersion relation, the field distribution, and the lifetime of the radiational eigenmodes in 2D PCs composed of metallic cylinders by means of the numerical simulation of the dipole radiation based on the FDTD method. Kuzmiak $et\ al.$ [27, 28] considered an 1D periodic array of alternating layers of vacuum$(\varepsilon = 1)$ and metal$\big(\varepsilon(\omega) = 1 - \omega_p^2/\omega^2\big)$. They employed the plane wave expansion and transfer matrix methods, and constructed an equivalent enlarged matrix to calculate the photonic band structures. They also calculated the 2D systems consisting of an infinite array of identical, infinitely long, parallel, metallic cylinders of circular cross section.

The plane wave expansion method is a straightforward method for the numerical calculation of dielectric PC band structures [29–31]. It expands the fields into the plane wave series, and leads to a finite matrix eigenvalue problem that can be readily solved by the standard LAPACK subroutines [32]. However, when it is applied to the M/D PCs, the eigenvalue equation is nonlinear and hard to solve. In this chapter, we develop an improved plane wave expansion method in order to make it suitable for the calculation of the M/D PCs' band structures [33, 34].

Within the classic theory, all the EM phenomena can be described by the system of Maxwell equations [35]. Based on these equations, we proposed an improved plane wave expansion method for the M/D PCs. This improved method is suitable equally to the 1D D/D PCs. Then we apply the improved method to the 1D M/D PC case in Sec.2, and calculate the photonic band structure of the corresponding 2D M/D sawtooth PCs. The photonic band structures and the corresponding DOS of cylindrical PCs are obtained in Sec.3.3 and Sec.3.4. Finally, we present the band structures of the square pillar and hole PCs, and compare the results with those of the cylinder and hole PCs.

1. Wave Equations and Eigen Modes of Photonic Crystals

The EM fields in mediums without free charges and currents can be described by the following Maxwell equations

$$\nabla \times \boldsymbol{E} + \frac{\partial \boldsymbol{B}}{\partial t} = 0, \tag{1}$$

$$\nabla \times \boldsymbol{H} - \frac{\partial \boldsymbol{D}}{\partial t} = 0, \tag{2}$$

$$\nabla \cdot \boldsymbol{B} = 0, \tag{3}$$

$$\nabla \cdot \boldsymbol{D} = 0, \tag{4}$$

where $\boldsymbol{E}$ and $\boldsymbol{H}$ are the electric and magnetic field, and $\boldsymbol{D}$ and $\boldsymbol{B}$ are the electric displacement and magnetic inductance, respectively. They are ralated by the constitutive equations

$$\boldsymbol{D} = \varepsilon(\boldsymbol{r})\boldsymbol{E}, \tag{5}$$

$$\boldsymbol{B} = \mu \boldsymbol{H}. \tag{6}$$

We seek harmonic solutions with a factor of $e^{-\mathrm{i}\omega t}$ for both $\boldsymbol{E}$ and $\boldsymbol{H}$ [21]

$$\boldsymbol{E}(\boldsymbol{r}, t) = \boldsymbol{E}(\boldsymbol{r})e^{-\mathrm{i}\omega t}, \tag{7}$$

$$\boldsymbol{H}(\boldsymbol{r}, t) = \boldsymbol{H}(\boldsymbol{r})e^{-\mathrm{i}\omega t}. \tag{8}$$

By expanding the fields $\boldsymbol{E}(\boldsymbol{r})$ and $\boldsymbol{H}(\boldsymbol{r})$ in plane waves, and eliminating $\boldsymbol{E}(\boldsymbol{r})$ or $\boldsymbol{H}(\boldsymbol{r})$ in Eq.(1)-(4), we can get a secular equation and the corresponding eigenmodes.

2. Plane Wave Expansion Method to the 1D D/D and M/D Photonic Crystals

The 1D PC model considered in this section is composed of layers A and B. Layer B is a dielectric medium with dielectric constant ε_2 and layer A is either a dielectric medium with dielectric constant ε_1 for the D/D PC, or a metallic medium for the M/D PC with the Drude type of dielectric function

$$\varepsilon_1(\omega) = \varepsilon_\infty - \frac{\omega_\mathrm{p}^2}{\omega^2}. \tag{9}$$

We choose the z axis perpendicular to the interface and the center of the layer A at z = 0. The thickness of layer A(B) is a_1 (a_2), so the structure period $d = a_1 + a_2$. We assume that the propagation direction of the EM wave is in the x–z plane and the field along the y axis is uniform.

2.1. TM Modes of D/D Photonic Crystal

For the TM mode, we expand the magnetic field in terms of Fourier series

$$\boldsymbol{H}(\boldsymbol{r}) = \sum_G C_G e^{\mathrm{i}[k_x x + (k+G)z]} \mathbf{i}_y, \tag{10}$$

where the reciprocal lattice vector $G = 2\pi n/d$ with $n = 0, \pm 1, \pm 2 \ldots$, k_x and k are the wave vectors in the x and z directions respectively. Hence the curl of $\boldsymbol{H}$ is

$$\nabla \times \boldsymbol{H}(\boldsymbol{r}) = \mathrm{i} \sum_G C_G e^{\mathrm{i}[k_x x + (k+G)z]} \left[k_x \mathbf{i}_z - (k+G)\mathbf{i}_x \right]. \tag{11}$$

For the 1D D/D PC with dielectric constants ε_1 and ε_2, $\frac{1}{\varepsilon(z)}$ can be expanded as

$$\frac{1}{\varepsilon(z)} = \sum_G \kappa(G) e^{\mathrm{i}Gz}, \tag{12}$$

with the Fourier factor

$$\kappa(G) = \frac{1}{d} \int_{-d/2}^{d/2} \frac{1}{\varepsilon(z)} e^{-\mathrm{i}Gz} dz = \begin{cases} \frac{1}{\varepsilon_1}\frac{a_1}{d} + \frac{1}{\varepsilon_2}\frac{a_2}{d}, & G = 0, \\ \left(\frac{1}{\varepsilon_1} - \frac{1}{\varepsilon_2}\right) \frac{1}{n\pi} \sin \frac{n\pi a_1}{d}, & G \neq 0. \end{cases} \tag{13}$$

From the Maxwell equations Eq.(1)-(4), we can get

$$\boldsymbol{E} = \frac{-1}{\omega \varepsilon_0 \varepsilon(z)} \sum_G C_G e^{\mathrm{i}[k_x x + (k+G)z]} \left[k_x \mathbf{i}_z - (k+G)\mathbf{i}_x \right], \tag{14}$$

and the secular equation

$$\sum_{G'} \kappa(G - G') \left[k_x^2 + (k+g)(k+G') \right] C_{G'} = \frac{\omega^2}{c^2} C_G. \tag{15}$$

Eq.(15) is a real symmetric eigenvalue equation. The band structure of D/D PC can be obtained from its eigenvalue ω^2/c^2.

However, for PC containing metallic medium with a frequency-dependent dielectric function, we can't get a secular equation according to the above procedure. For this case we propose an improved plane wave expansion method [33].

By inspecting Eq.(2) and the expression of $\nabla \times \boldsymbol{H}$ Eq.(11), we let

$$\boldsymbol{E} = \sum_G D_G e^{\mathrm{i}[k_x x+(k+G)z]} \left[k_x \mathbf{i}_z - (k+G)\mathbf{i}_x\right], \tag{16}$$

so its curl is

$$\begin{aligned} \nabla \times \boldsymbol{E} &= -\mathrm{i}\sum_G D_G e^{\mathrm{i}[k_x x+(k+G)z]} \left[k_x^2 + (k+G)^2\right] \mathrm{i}_y \\ &= \mathrm{i}\omega\mu_0 \sum_G C_G e^{\mathrm{i}[k_x x+(k+G)z]} \mathbf{i}_y, \end{aligned} \tag{17}$$

Comparing Eqs.(16) and (17) we obtain the coefficient

$$D_G = -\frac{\omega\mu_0}{k_x^2 + (k+G)^2} C_G. \tag{18}$$

Then from

$$\nabla \times \boldsymbol{H} = -\mathrm{i}\omega\varepsilon_0\varepsilon(z)\boldsymbol{E}, \tag{19}$$

$$\nabla \times (\nabla \times \boldsymbol{H}) = \sum_G C_G e^{\mathrm{i}[k_x x+(k+G)z]} \left[k_x^2 + (k+G)^2\right] \mathbf{i}_y, \tag{20}$$

We obtain the secular equation

$$\left[k_x^2 + (k+G)^2\right] C_G = \left(\frac{\omega}{c}\right)^2 \sum_{G'} A_{kg}\varepsilon(G-G')C_{G'}, \tag{21}$$

where

$$A_{kg} = \left[\frac{k_x^2 + (k+G)\left(k+G'\right)}{k_x^2 + (k+G')^2}\right], \tag{22}$$

$$\begin{aligned} \varepsilon(G) &= \frac{1}{d}\int_{-d/2}^{d/2} \varepsilon(z) e^{-\mathrm{i}Gz} dz \\ &= \begin{cases} \left(\varepsilon_1 \frac{a_1}{d} + \varepsilon_2 \frac{a_2}{d}\right), & G = 0, \\ (\varepsilon_1 - \varepsilon_2) \frac{1}{n\pi} \sin \frac{n\pi a_1}{d}, & G \neq 0. \end{cases} \end{aligned} \tag{23}$$

Eq.(21) is a real non-symmetric eigenvalue equation, which can be readily solved by the LAPACK package. Then the band structures of the TM modes for the M/D PCs can be obtained without solving the nonlinear equation.

The band structure of the TM modes for 1D D/D PC by the traditional and improved plane wave expansion methods is shown in Fig.1(a) and Fig.1(b), where $\varepsilon_1 = 2$ and $\varepsilon_2 = 1, a_1/d = 0.6$. The unit of the frequency is $d/2\pi c$, and the unit of the wave vector k is $2\pi/d$, these are used throughout this work. The points Γ, Z, L, and X represent the special k points (0, 0), (0, 0.5), (0.5, 0.5), and (0.5, 0) in the first Brillouin zone, respectively(see the inset of Fig.1(a)). No band gap exists among the five lowest bands. The agreement between Fig.1(a) and Fig.1(b) is good, which means these two methods are consistent.

Besides the photonic band structure, the distribution of the EM field of the corresponding eigenmodes can also be obtained. The time-averaged EM energy density $U_{kn}(\boldsymbol{\rho})$ reads

$$U_{kn}(\boldsymbol{\rho}) = \frac{1}{4}\left[\varepsilon_0\varepsilon(\boldsymbol{\rho})\left|\boldsymbol{E}_{kn}(\boldsymbol{\rho})\right|^2 + \mu_0\left|\boldsymbol{H}_{kn}(\boldsymbol{\rho})\right|^2\right], \tag{24}$$

where, $\boldsymbol{\rho}$ is the position vextor with $\boldsymbol{\rho} = x\mathrm{i}_{\boldsymbol{x}} + y\mathrm{i}_{\boldsymbol{y}} + z\mathrm{i}_{\boldsymbol{z}}$

The EM field $U_{kn}(\boldsymbol{\rho})$ distributions in the 1D D/D PC of the lowest 5 modes at $k_x = 0.1, k = 0.1$ are plotted in Fig.2(a). The EM energies are concentrated in the dielectric layer with a larger dielectric constant.

2.2. TM Modes of M/D Photonic Crystal

The secular equation (21) also applies to the M/D PC case with

$$\begin{aligned}\varepsilon(G) &= \frac{1}{d}\int_{-d/2}^{d/2}\varepsilon(z)e^{-\mathrm{i}Gz}dz \\ &= \begin{cases}\left(\varepsilon_\infty\frac{a_1}{d} + \varepsilon_2\frac{a_2}{d}\right) - \frac{\omega_\mathrm{p}^2}{\omega^2}\frac{a_1}{d}, & G = 0, \\ \left[(\varepsilon_\infty - \varepsilon_2) - \frac{\omega_\mathrm{p}^2}{\omega^2}\right]\frac{1}{n\pi}\sin\frac{n\pi a_1}{d}, & G \neq 0.\end{cases}\end{aligned} \tag{25}$$

Inserting Eq.(25) into Eq.(21), we obtain the secular equation as

$$\left[k_x^2 + (k+G)^2\right]C_G + \left(\frac{\omega_\mathrm{p}}{c}\right)^2\sum_{G'}A_{kg}\varepsilon''\left(G - G'\right)C_{G'} = \left(\frac{\omega}{c}\right)^2\sum_{G'}A_{kg}\varepsilon'\left(G - G'\right)C_{G'}, \tag{26}$$

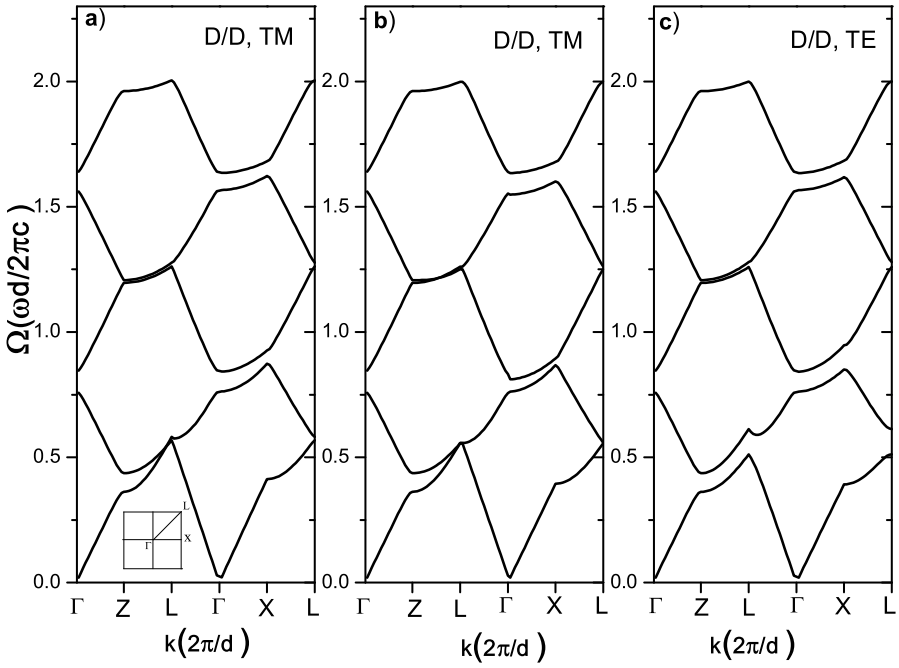

Figure 1. Band structures of the lowest five eigenmodes for the D/D photonic crystal ($\varepsilon_1 = 2, \varepsilon_2 = 1, a_1/d = 0.6$). The points Γ, Z, L, and X represent the special k points (0, 0), (0, 0.5), (0.5, 0.5), and (0.5, 0) in the first Brillouin zone. a): TM modes using secular equation as Eq.(15). b): TM modes using secular equation (21). c): TE modes.

where A_{kg} is given in Eq.(22), and

$$\varepsilon'(G) = \begin{cases} \left(\varepsilon_\infty \frac{a_1}{d} + \varepsilon_2 \frac{a_2}{d}\right), & G = 0, \\ (\varepsilon_\infty - \varepsilon_2) \frac{1}{n\pi} \sin \frac{n\pi a_1}{d}, & G \neq 0. \end{cases} \tag{27}$$

$$\varepsilon''(G) = \begin{cases} a_1/d, & G = 0, \\ \frac{1}{n\pi} \sin \frac{n\pi a_1}{d}, & G \neq 0. \end{cases} \tag{28}$$

The band structure of the TM modes for the 1D M/D PC is plotted in Fig.3(a), with parameters: $\varepsilon_\infty = 1, \varepsilon_2 = 2, a_1/d = 0.5$, $\Omega_{\rm p} = \frac{\omega_{\rm p} d}{2\pi c} = 1$.

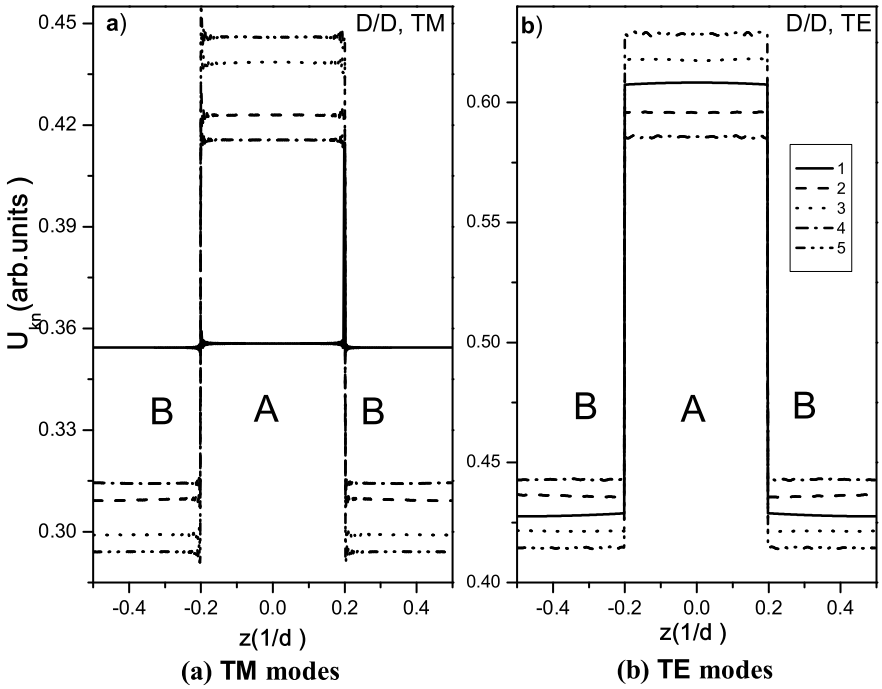

Figure 2. Distribution of EM field energy of the lowest five eigenmodes of the 1D D/D photonic crystal ($\varepsilon_1 = 2, \varepsilon_2 = 1, a_1/d = 0.6, k_x = k = 0.1$). a):TM modes. b)TE modes. The energy units of a) and b) are the same.

Comparing Fig.3(a) with the D/D PC case in Fig.1(a), for the M/D PCs, there is a large band gap between the lowest band and $\Omega_{\rm p} = 0$ ($\Delta\Omega \approx 0.5$). The lowest two modes are relatively flat, which means that the group velocities of these two modes are small and different optical enhancement can be expected. This property can be used to the development of efficient optical devices [21]. The eigen-frequencies of the lowest two modes are all smaller than $\Omega_{\rm p} = 1$, which means the dielectric function $\varepsilon_1(\omega)$ is negative for these two modes, i.e. the metal layer acts as the absorption layer for the EM field. The EM field distributions for the lowest 5 modes at $k_x = 0.1, k = 0.1$ are shown in Fig.4(a). The energy densities oscillate near the interface, and the magnitudes decay with the distance from the interface. These features are in accordance with the property

of the surface plasmon mode [36]. It means surface plasmon modes exist near the interface. As the eigen-frequency is smaller than $\Omega_{\rm p}$, the energy of the first mode is negative in the metal layer, which leads to the absorption of the EM field energy.

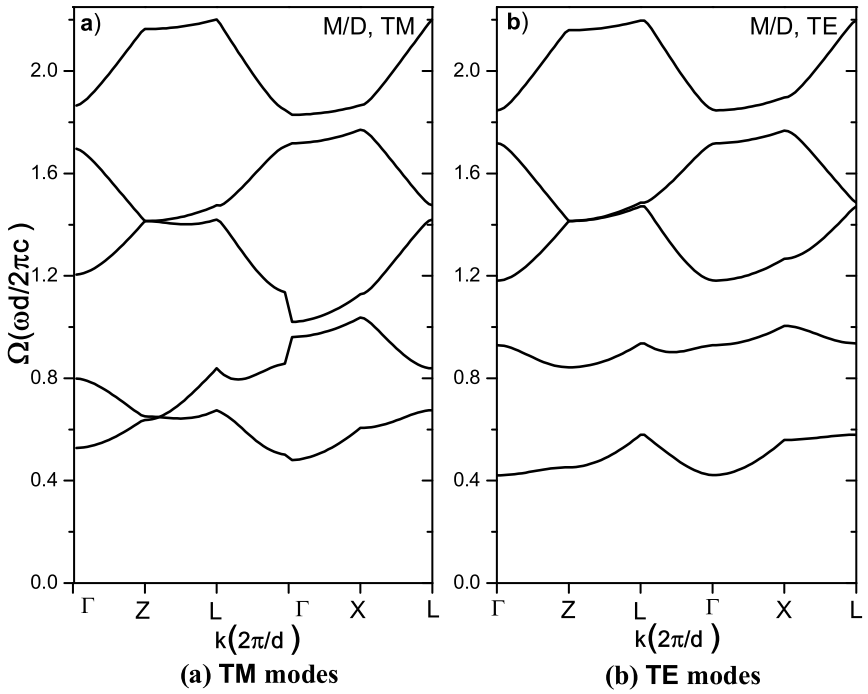

Figure 3. Band structure of the lowest five eigenmodes of the 1D M/D photonic crystal ($\varepsilon_\infty = 1, \varepsilon_2 = 2, a_1/d = 0.5$). a)TM modes. b)TE modes.

2.3. TE Modes of D/D Photonic Crystal

We expand the electric field as

$$\boldsymbol{E}=\sum_G C_G e^{\mathrm{i}[k_x x+(k+G)z]}\mathbf{i}_y, \tag{29}$$

the magnetic field $\boldsymbol{H}$ and its curl $\nabla \times \boldsymbol{H}$ can be obtained as

$$\boldsymbol{H} = \frac{1}{\mu_0}\frac{1}{\mathrm{i}\omega}\nabla \times \boldsymbol{E} = \frac{1}{\mu_0\omega}\sum_G C_G e^{\mathrm{i}[k_x x+(k+G)z]}\left[k_x \mathbf{i}_z - (k+G)\,\mathbf{i}_x\right], \quad (30)$$

$$\nabla \times \boldsymbol{H} = \frac{\text{-i}}{\mu_0\omega}\sum_G C_G e^{\mathrm{i}[k_x x+(k+G)z]}\left[k_x^2 + (k+G)^2\right]\mathbf{i}_y = -\mathrm{i}\omega\varepsilon_0\varepsilon\,(z)\,\boldsymbol{E}. \quad (31)$$

From Eq.(2) we get the secular equation

$$\left[k_x^2 + (k+G)^2\right] C_G = \frac{\omega^2}{c^2}\sum_{G'}\varepsilon\left(G-G'\right)C_{G'}, \quad (32)$$

where $\varepsilon\,(G)$ is given in Eq.(23). The band structure of the TE modes for the D/D PC is shown in Fig.1(c) with parameters: $\varepsilon_1 = 2, \varepsilon_2 = 1, a_1/d = 0.6$. The EM field distributions for the lowest 5 modes at $k_x = 0.1, k = 0.1$ are shown in Fig.2(b). We found that the band structures are similar to the 1D D/D photonic crystals, and the EM energies are concentrated in dielectric layer with larger dielectric constant.

2.4. TE Modes of M/D Photonic Crystal

Except for the Fourier component of $\varepsilon(z)$, the secular equation (32) of the TE modes for the D/D PC is also applicable to the M/D PC case. By inserting Eq.(25) into Eq.(32), we obtain the secular equation

$$\left[k_x^2 + (k+G)^2\right] C_G + \frac{\omega_{\mathrm{p}}^2}{c^2}\sum_{G'}\varepsilon''(G-G')C_{G'} = \frac{\omega^2}{c^2}\sum_{G'}\varepsilon'(G-G')C_{G'}, \quad (33)$$

where $\varepsilon'(G)$ and $\varepsilon''(G)$ are given in Eq.(27) and (28), respectively.

In Fig.3(b), the band structure of the TE modes for the M/D PC is plotted with parameters: $\varepsilon_\infty = 1, \varepsilon_2 = 2, a_1/d = 0.5$ and $\Omega_{\mathrm{p}} = 1$. Similar to the TM modes of the 1D M/D photonic crystal in Fig.3(b), there exists a wide band gap ($\Delta\Omega = 0.4$) between the lowest band and $\Omega = 0$. The lowest two bands are relatively flat. Fig.4(b) shows the energy densities for the lowest 5 bands at $k_x = 0.1, k = 0.1$. The EM energies are mainly concentrated in the dielectric layer, which is more evident in the lowest two modes. The energies distribute

evenly in both layers, and do not decay from the M/D interface. So no plasmon mode exists for the TE modes.

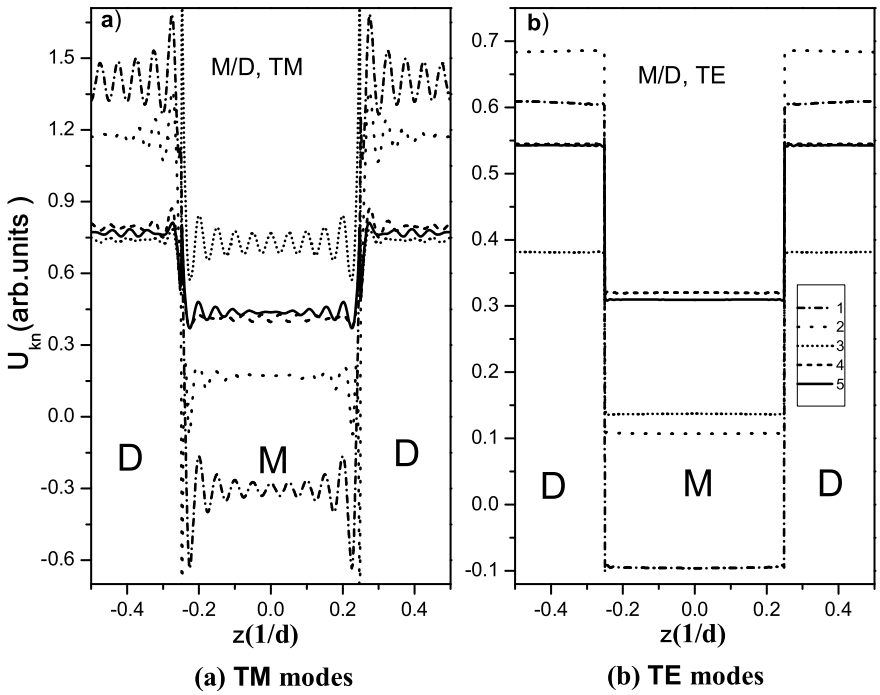

Figure 4. EM field distribution of the lowest five eigenmodes for the M/D PC ($\varepsilon_\infty = 1, \varepsilon_2 = 2, a_1/d = 0.5, k_x = k = 0.1$). a)TM modes. b)TE modes. The energy units of a) and b) are the same.

The above photonic band structures of the M/D (see Fig.3) and D/D (see Fig.1) PCs show that the metallic medium can induce more band gaps, which is more attractive for the development of photonic devices.

3. Photonic Band Structure of the 2D M/D Photonic Crystals

There are various types of 2D PCs, in this section we apply the above improved plane wave expansion method to the sawtooth, cylinder and hole 2D PCs. As

shown in Fig.5 the cross section of the unit cell for these two structures are assumed to be in the $x-z$ plane, and the periods in the z and x directions are d and b respectively. In this figure, I represents the metallic medium with the dielectric functions $\varepsilon_1(\omega)$ of Eq.(9), II represents the dielectric medium with a constant ε_2. For the 2D hole PCs, the I and II exchange.

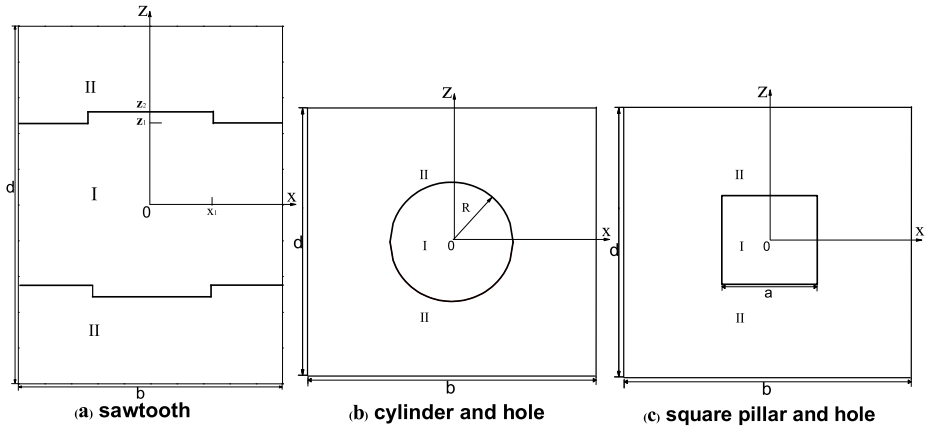

Figure 5. Cross section geometry of the unit cells of the 2D M/D PCs.

3.1. TE Modes of M/D Sawtooth Photonic Crystal

First we expand the electric field as

$$\boldsymbol{E}=\sum_{\boldsymbol{G}}C_{\boldsymbol{G}}\mathrm{e}^{\mathrm{i}(\boldsymbol{k}+\boldsymbol{G})\cdot\boldsymbol{\rho}}\mathbf{i}_y, \tag{34}$$

with $\boldsymbol{\rho}$ and $\boldsymbol{k}+\boldsymbol{G}$ in the $x-z$ plane.

$$\boldsymbol{\rho}=x\mathbf{i}_x+z\mathbf{i}_z,$$

$$\boldsymbol{k}+\boldsymbol{G}=(k_x+F)\mathbf{i}_x+(k+G)\mathbf{i}_z.$$

$\boldsymbol{k}$ is the wave vector in the first Brillouin zone ($\boldsymbol{k}=k_x\mathbf{i}_x+k\mathbf{i}_z$), $\boldsymbol{G}$ is the reciprocal lattice vector ($\boldsymbol{G}=F\mathbf{i}_x+G\mathbf{i}_z$, $G=2\pi m/d, F=2\pi n/b$ with

$m = 0, \pm1, \pm2, \ldots; n = 0, \pm1, \pm2, \ldots$), and d and b are the periods in the z and x directions respectively. The magnetic field can be obtained as

$$\begin{aligned} \boldsymbol{H} &= \frac{1}{\mu_0}\frac{1}{\mathrm{i}\omega}\nabla \times \boldsymbol{E} \\ &= \frac{1}{\mu_0\omega}\sum_{\boldsymbol{G}} C_{\boldsymbol{G}} \mathrm{e}^{\mathrm{i}(\boldsymbol{k}+\boldsymbol{G})\cdot\boldsymbol{\rho}}(\boldsymbol{k}+\boldsymbol{G}) \times \mathbf{i}_y, \end{aligned} \tag{35}$$

From the Maxwell equations, we can get the secular equation

$$(\boldsymbol{k}+\boldsymbol{G})^2 C_{\boldsymbol{G}} = \frac{\omega^2}{c^2}\sum_{\boldsymbol{G}'} \varepsilon(\boldsymbol{G}-\boldsymbol{G}')C_{\boldsymbol{G}'}, \tag{36}$$

where $\varepsilon(\boldsymbol{G})$ is the 2D Fourier component of $\varepsilon(\boldsymbol{\rho})$,

$$\varepsilon(\boldsymbol{G}) = \frac{1}{db}\int_{-d/2}^{d/2}\mathrm{d}z\int_{-b/2}^{b/2}\mathrm{d}x\varepsilon(\boldsymbol{\rho})\mathrm{e}^{-\mathrm{i}(Fx+Gz)}. \tag{37}$$

For the sawtooth type PCs shown in Fig.5(a), the Fourier component of $\varepsilon(\boldsymbol{\rho})$ can be written as

$$\varepsilon_{m,n} = \begin{cases} X_2[\varepsilon_1 Z_1 + \varepsilon_2(1-Z_1)] + X_1[\varepsilon_1 Z_2 + \varepsilon_2(1-Z_2)], \\ (\varepsilon_1-\varepsilon_2)[(1-X_1)\sin\pi m Z_1 + X_1 \sin\pi m Z_2]/(\pi m), \\ (\varepsilon_1-\varepsilon_2)\sin\pi n X_1(Z_2 - Z_1)/\pi n, \\ (\varepsilon_1-\varepsilon_2)\sin\pi n X_1(\sin\pi m Z_2 - \sin\pi m Z_1)/(\pi^2 mn), \end{cases} \tag{38}$$

The four formulas in Eq.(38) correspond to ①$m = n = 0$; ②$m \neq 0, n = 0$; ③$m = 0, n \neq 0$ and ④$m \neq 0, n \neq 0$, respectively. And

$$X_1 = 2x_1/b, X_2 = 1 - X_1, Z_1 = 2z_1/d, Z_2 = 2z_2/d.$$

For the M/D PCs, by inserting the metal dielectric function Eq.(9) into Eq.(36), we can get the secular equation

$$(\boldsymbol{k}+\boldsymbol{G})^2 C_{\boldsymbol{G}} + \frac{\omega_\mathrm{p}^2}{c^2}\sum_{\boldsymbol{G}'}\varepsilon''(\boldsymbol{G}-\boldsymbol{G}')C_{\boldsymbol{G}'} = \frac{\omega^2}{c^2}\sum_{\boldsymbol{G}'}\varepsilon'(\boldsymbol{G}-\boldsymbol{G}')C_{\boldsymbol{G}'}, \tag{39}$$

where $\varepsilon'(\boldsymbol{G})$ and $\varepsilon''(\boldsymbol{G})$ are $\varepsilon_{m,n}$ in Eq.(38) by setting $\varepsilon_1 = \varepsilon_\infty, \varepsilon_2 = 2$, and $\varepsilon_1 = 1, \varepsilon_2 = 0$ respectively.

The photonic bands from the Γ to the X point as functions of k_x for the 2D M/D sawtooth PC are shown in Fig.6(a), with parameters: $\varepsilon_\infty = 1, \varepsilon_2 = 2, X_1 = 0.5, Z_1 = 0.4, Z_2 = 0.5, d/b = 2, \Omega_{\rm p} = (\omega_{\rm p} d/2\pi c) = 1$. The corresponding 1D PC case of $Z_0 = a_1/d = 0.45$ is shown in Fig.6(b), where a_1 is the thickness of the metallic layer. The band structure of this 2D PC can be well represented by folding that of 1D PC at $k_x = \pi/b = 2\pi/d$. There is a large band gap between the lowest band and $\Omega = 0$ ($\Delta\Omega = 0.395$). The lowest two bands of the 2D M/D case are relatively flat with $\Omega < \Omega_{\rm p}$, i.e. for these two modes the dielectric constant of metal is negative.

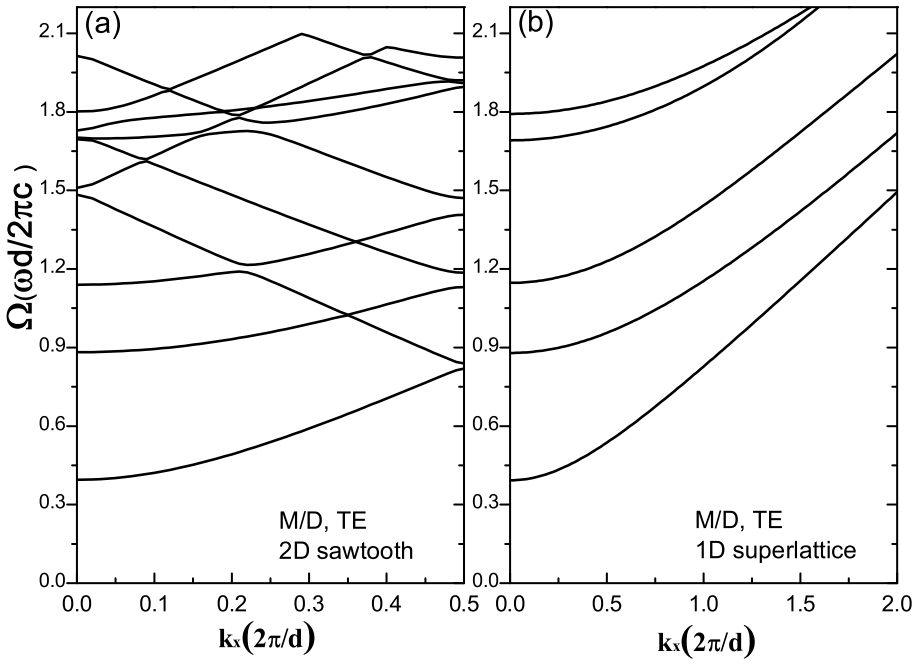

Figure 6. Band structure of the TE modes of $\varepsilon_\infty = 1, \varepsilon_2 = 2, d/b = 2, \Omega_{\rm p} = 1$ for: (a) 2D M/D sawtooth PC($X_1 = 0.5, Z_1 = 0.4, Z_2 = 0.5$), (b) the corresponding 1D PC($a_1/d = 0.45$).

3.2. TM Modes of M/D Sawtooth Photonic Crystal

For the 2D PC case, the expressions of $\nabla \times \boldsymbol{H}$ and its curl are

$$\nabla \times \boldsymbol{H} = -\mathrm{i}\omega\varepsilon_0\varepsilon(\boldsymbol{\rho})\boldsymbol{E}, \tag{40}$$

$$\nabla \times (\nabla \times \boldsymbol{H}) = \sum_{\boldsymbol{G}} C_{\boldsymbol{G}} \mathrm{e}^{\mathrm{i}(\boldsymbol{k}+\boldsymbol{G})\cdot\boldsymbol{\rho}} (\boldsymbol{k}+\boldsymbol{G})^2 \mathrm{i}_y, \tag{41}$$

while $\boldsymbol{E}$ and its curl become

$$\boldsymbol{E} = \sum_{\boldsymbol{G}} D_{\boldsymbol{G}} \mathrm{e}^{\mathrm{i}(\boldsymbol{k}+\boldsymbol{G})\cdot\boldsymbol{\rho}} (\boldsymbol{k}+\boldsymbol{G}) \times \mathrm{i}_y, \tag{42}$$

$$\begin{aligned} \nabla \times \boldsymbol{E} &= -\mathrm{i}\sum_{\boldsymbol{G}} D_{\boldsymbol{G}} \mathrm{e}^{\mathrm{i}[k_x x + (k+G)z]} \left[k_x^2 + (k+G)^2\right] \mathrm{i}_y \\ &= \mathrm{i}\omega\mu_0 \sum_{\boldsymbol{G}} C_{\boldsymbol{G}} \mathrm{e}^{\mathrm{i}(\boldsymbol{k}+\boldsymbol{G})\cdot\boldsymbol{\rho}} (\boldsymbol{k}+\boldsymbol{G})^2 \mathrm{i}_y. \end{aligned} \tag{43}$$

From Eq.(40), (41) and (43), we get

$$D_{\boldsymbol{G}} = -\frac{\omega\mu_0}{(\boldsymbol{k}+\boldsymbol{G})^2} C_{\boldsymbol{G}}. \tag{44}$$

and

$$(\boldsymbol{k}+\boldsymbol{G})^2 C_{\boldsymbol{G}} = \left(\frac{\omega}{c}\right)^2 \sum_{\boldsymbol{G}'} B_{kg}\varepsilon(\boldsymbol{G}-\boldsymbol{G}') C_{\boldsymbol{G}'}, \tag{45}$$

where,

$$B_{kg} = \frac{(\boldsymbol{k}+\boldsymbol{G})\cdot(\boldsymbol{k}+\boldsymbol{G}')}{(\boldsymbol{k}+\boldsymbol{G}')^2}. \tag{46}$$

For the metal dielectric function of Eq.(9), the following secular equation can be obtained

$$(\boldsymbol{k}+\boldsymbol{G})^2 C_{\boldsymbol{G}} + \left(\frac{\omega_\mathrm{p}}{c}\right)^2 \sum_{\boldsymbol{G}'} B_{kg}\varepsilon''\left(\boldsymbol{G}-\boldsymbol{G}'\right) C_{\boldsymbol{G}'} = \left(\frac{\omega}{c}\right)^2 \sum_{\boldsymbol{G}'} B_{kg}\varepsilon'\left(\boldsymbol{G}-\boldsymbol{G}'\right) C_{\boldsymbol{G}'}, \tag{47}$$

where $\varepsilon'(\boldsymbol{G})$ and $\varepsilon''(\boldsymbol{G})$ are given in Eq.(38) in the same way as in Eq.(39).

The photonic bands from the Γ to the X point as functions of k_x for the 2D M/D sawtooth PC are shown in Fig.7, with parameters: $\varepsilon_\infty = 1, \varepsilon_2 = 2, X_1 = 0.5, Z_1 = 0.4, Z_2 = 0.5, d/b = 2, \Omega_\mathrm{p} = (\omega_\mathrm{p} d/2\pi c) = 1$. Comparing Fig.7 with the TE modes in Fig.6(a), band structures of TE and TM modes are similar.

There is a larger band gap between the lowest band and $\Omega = 0(\Delta\Omega = 0.538)$. The bands of the lowest two modes are relatively flat with $\Omega < \Omega_{\rm p}$, which means for these two modes the dielectric constant of the metal is negative.

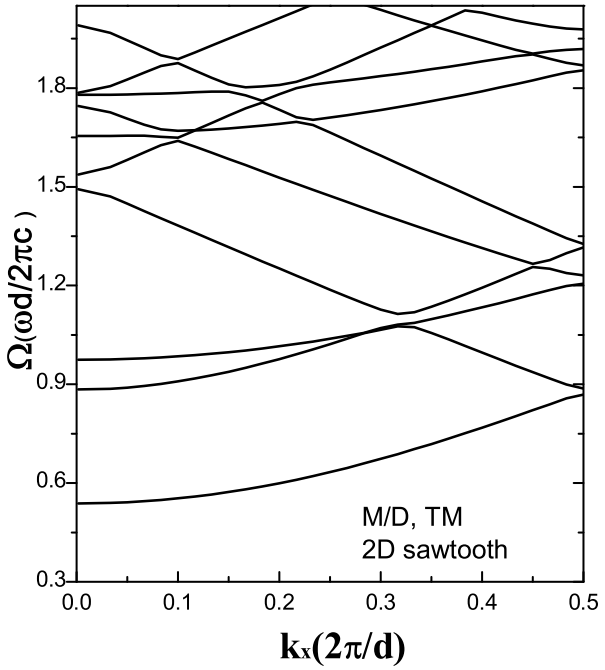

Figure 7. Band structures of the TM modes for the 2D M/D sawtooth PC of $\varepsilon_\infty = 1, \varepsilon_2 = 2, X_1 = 0.5, Z_1 = 0.4, Z_2 = 0.5, d/b = 2, \Omega_{\rm p} = 1$.

3.3. TE Modes of M/D Cylinder and Hole Photonic Crystals

Since Ebbesen $et\ al$ [37] found the extraordinary optical transmission in the 2D PCs of holes in metallic medium, the optical properties of the cylinder and hole PCs have became attractive in the optics research area. In this section we calculate the band structuress of cylinder and hole PCs as well as the corresponding DOS. The latter was calculated according to Ref. [19].

Fig.5(b) shows the cross section geometry for the unit cell of the cylinder, where I and II are metal and dielectric mediums, respectively. For the hole PCs,

the I and II exchange. The secular equations of the TE modes for these two 2D PCs are the same as Eq.(36) except for the Fourier component of the dielectric function, which reads

$$\begin{aligned} \varepsilon(\boldsymbol{G}) &= \frac{1}{db}\int_{-d/2}^{d/2}\int_{-b/2}^{b/2}\mathrm{d}\boldsymbol{\rho}\varepsilon(\boldsymbol{\rho})\mathrm{e}^{-\mathrm{i}\boldsymbol{G}\cdot\boldsymbol{\rho}} \\ &= \begin{cases} \varepsilon_1 X + \varepsilon_2(1-X), & G = 0, \\ (\varepsilon_1-\varepsilon_2)\frac{2\pi}{db}\int_0^R \rho\mathrm{d}\rho J_0(G\rho), & G \neq 0. \end{cases} \end{aligned} \tag{48}$$

where $X = (\pi R^2/db)$ is the filling factor.

Fig.8 shows the band structures and the corresponding DOS of the TE modes for the 2D M/D cylinder and hole PCs with parameters: $\varepsilon_\infty = 1, R/d = 0.2, d/b = 0.9, \Omega_\mathrm{p} = 1$. The band structure and DOS of the cylinder case with $\varepsilon_2 = 2$ are given in Fig.8(a). There exist a band gap between the lowest band and $\Omega = 0(\Delta\Omega = 0.194)$, the corresponding DOS is zero on the right. In addition, there are partial band gaps in the Γ–Z, L–Γ, and Γ–X directions between the lowest two bands, the DOS values at these Ω regions are close to zero. There are 7 photonic bands with $\Omega < \Omega_\mathrm{p}$, thus for these modes the dielectric constant of metal is negative. Fig.8(b) shows the band structure and DOS of the hole case with $\varepsilon_1 = 2$, which has different features from Fig.8(a). There is a wide band gap between the lowest two bands with $\Delta\Omega = 0.307$, which is not transparent for light. The lowest two bands are extremely flat, which means the group velocities of these two modes are small and different optical enhancement can be expected. This property can be used to the development of efficient optical devices [21]. The band gap between the lowest band and $\Omega = 0$ is $\Delta\Omega \approx 0.75$, which is larger than the cylinder case.

3.4. TM Modes of M/D Cylinder and Hole Photonic Crystals

For this case the secular equation is the same as Eq.(45) with the Fourier component of the dielectric function given in Eq.(48).

The band structures and DOS of the TM modes for the 2D M/D cylinder and hole PCs are shown in Fig.9 with parameters: $\varepsilon_\infty = 1, R/d = 0.2, d/b = 0.9, \Omega_\mathrm{p} = 1$. Fig.9(a) presents the band structure of the cylinder case with $\varepsilon_2 = 2$. The band structures of TM and TE modes are similar, except for the large band gap between the lowest band and $\Omega = 0(\Delta\Omega = 0.215)$. Fig.9(b) gives the band structure of the hole case with $\varepsilon_1 = 2$. As in Fig.8(b), there is only one frequency band with $\Omega < \Omega_\mathrm{p}$, and the band gap between the lowest

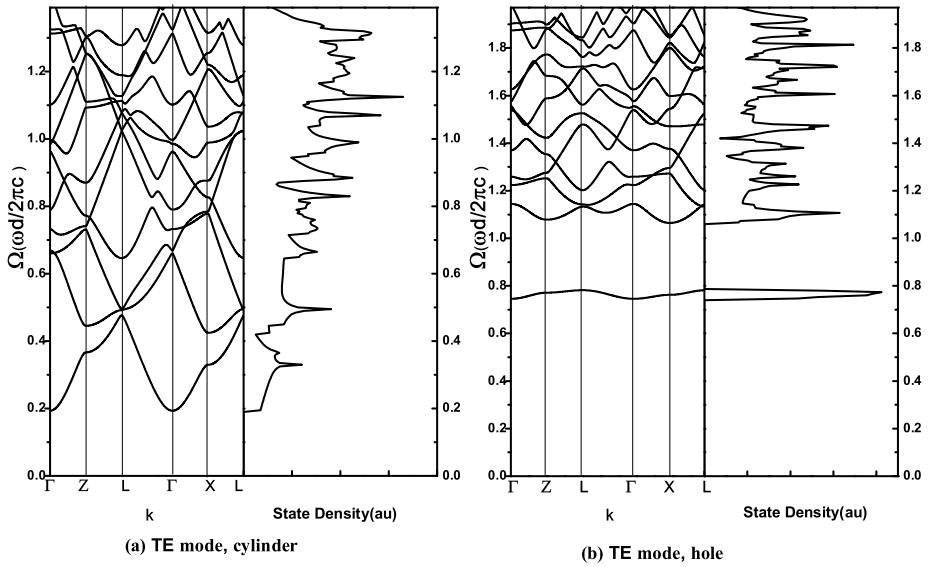

Figure 8. Band structures and DOS of the TE modes. a) 2D M/D cylinder ($\varepsilon_\infty = 1, \varepsilon_2 = 2$) b) hole ($\varepsilon_\infty = 1, \varepsilon_1 = 2$) PCs with $R/d = 0.2, d/b = 0.9, \Omega_\mathrm{p} = 1$.

band and $\Omega = 0$ is $\Delta\Omega = 0.81$. While the band gap between the lowest two bands does not exist.

By comparing the band structures in Fig.8 with that in Fig.9, we found that for both the cylinder and the hole type M/D PCs, there exists a large band gap between the lowest band and $\Omega = 0$.

3.5. Eigen Modes of M/D Square Pillar and Hole Photonic Crystals

In order to study the effect of the cylinder and hole shape on the optical property of the M/D PCs, we calculate the band structures of square pillar and hole PCs

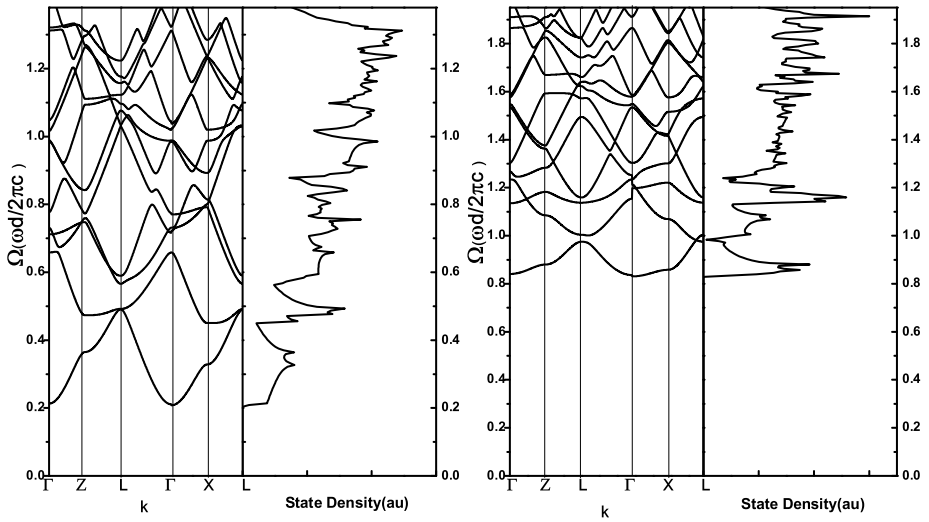

Figure 9. Band structures and DOS of the TM modes. a) 2D M/D cylinder ($\varepsilon_\infty = 1, \varepsilon_2 = 2$) b) hole ($\varepsilon_\infty = 1, \varepsilon_1 = 2$) PCs with $R/d = 0.2, d/b = 0.9, \Omega_{\rm p} = 1$.

shown in Fig.5(c). The Fourier component of $\varepsilon(\boldsymbol{\rho})$ can be written as

$$\varepsilon_{m,n} = \frac{1}{db}\int_{-\frac{b}{2}}^{\frac{b}{2}}\int_{-\frac{b}{2}}^{\frac{b}{2}} \varepsilon(\boldsymbol{\rho}) \mathrm{e}^{-\mathrm{i}(Fx+Gz)} \mathrm{d}z\mathrm{d}x = \begin{cases} \varepsilon_1 \frac{a^2}{db} + \varepsilon_2(1-\frac{a^2}{db}), \\ \frac{(\varepsilon_1-\varepsilon_2)a}{m\pi d} \sin\frac{m\pi a}{b}, \\ \frac{(\varepsilon_1-\varepsilon_2)a}{n\pi b} \sin\frac{n\pi a}{d}, \\ \frac{(\varepsilon_1-\varepsilon_2)a}{mn\pi^2} \sin\frac{n\pi a}{d} \sin\frac{m\pi a}{b}, \end{cases} \tag{49}$$

for ①$m = n = 0$; ②$m \neq 0, n = 0$; ③$m = 0, n \neq 0$ and ④$m \neq 0, n \neq 0$, respectively.

The secular equations of TE and TM modes for these two PCs are the same as Eq.(36) and (45) respectively. $\varepsilon'(\boldsymbol{G})$ and $\varepsilon''(\boldsymbol{G})$ in Eq.(47) are given in Eq.(49). For the square pillar, $\varepsilon'(\boldsymbol{G})$ and $\varepsilon''(\boldsymbol{G})$ are $\varepsilon_{m,n}$ in Eq.(49) for the case of $\varepsilon_1 = \varepsilon_\infty, \varepsilon_2 = 2$ and $\varepsilon_1 = 1, \varepsilon_2 = 0$ respectively. While for the square hole, $\varepsilon'(\boldsymbol{G})$ and $\varepsilon''(\boldsymbol{G})$ can be obtained by setting $\varepsilon_2 = \varepsilon_\infty, \varepsilon_1 = 2$ and

$\varepsilon_2 = 1, \varepsilon_1 = 0$ respectively.

The band structures of TE modes for the square pillar and hole PCs are shown in Fig.10(a), with parameters $\varepsilon_\infty = 1, a/d = 0.2\sqrt{\pi}, d/b = 0.9, \Omega_\mathrm{p} = 1$. The cross section areas of the square pillar($\varepsilon_2 = 2$) and hole($\varepsilon_1 = 2$) PCs are set to be equal to cylinder and hole cases respectively. By comparing Fig.8 with Fig.10(a), we found that the band structure of square and circular PCs are very similar when the cross section areas are equal($\pi R^2 = a^2$). The band structure of TM modes for the square pillar and hole PCs are shown in Fig.10(b), parameters are the same with the TE modes. Comparison between Fig.9 and Fig.10(b) shows that the band structure of TM modes for square and circular PCs are very similar when the cross section areas are equal. Therefore, the band structure is insensitive to the cross section shape for the same area.

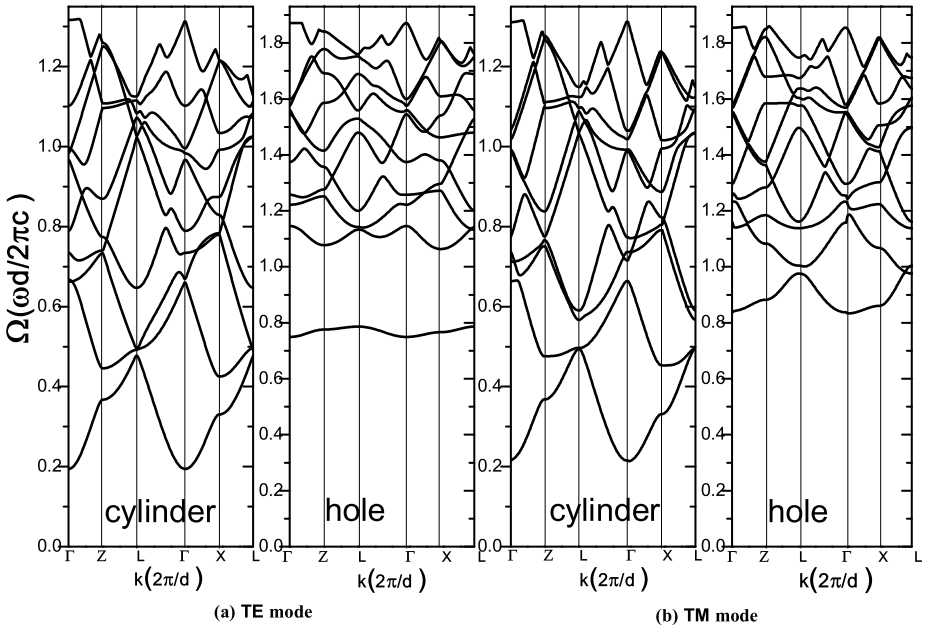

Figure 10. Band structures of the eigen modes for the 2D M/D square pillar, ($\varepsilon_\infty = 1, \varepsilon_2 = 2$) and hole ($\varepsilon_\infty = 1, \varepsilon_1 = 2$) PCs with $a/d = 0.2\sqrt{\pi}, d/b = 0.9, \Omega_\mathrm{p} = 1$. a) TE modes. b) TM modes.

Conclusion

For the numerical analysis of the photonic band structures of the M/D PCs, an improved plane wave expansion method was proposed in detail in this chapter and applied to several M/D PC configurations. The main advantage of this method is that it can avoid solving nonlinear eigenvalue equation when calculating the band structure of M/D PCs, and it is applicable to both D/D and M/D PCs. This improved method was first applied to the 1D D/D PCs, and the results of this method are consistent with the traditional one, which proved its correctness.

The results indicate that all the M/D PC configurations we choose show a relatively wide band gap between the lowest mode and $\Omega = 0$, which can be used to control the propagation of light. The photonic band structures of the 1D D/D and M/D PCs show that the M/D PCs can get a band gap more easily than the D/D ones, so the PCs containing metallic medium is more attractive. For the 2D cylinder and hole PCs, the band structures are similar. However, the lowest two bands of hole PC are flat, which means the group velocities of these two modes are small and different optical enhancement can be expected. This property can be used to the development of efficient optical device [21]. The hole PC exhibits a larger band gap than the cylinder one, which is more useful in the control of light propagation. Comparison between the circular and square pillar and hole PCs shows that the shape influence on the band structure is small when the cross section areas of both PCs are equal.

Acknowledgments

This work was supported by the special funds for the National Basic Research Program of China (Grant No. 2011CB922200). Especially, we want to thank the help of Dr. Haibin Wu in our research team.

References

[1] Yablonovitch, E. *Phys. Rev. Lett.* 1987, 58, 2059-2062.

[2] John, S. *Phys. Rev. Lett.* 1987, 58, 2486-2489.

[3] Joannopoulos, J. D.; Villeneuve, P. R.; Fan, S. *Nature* 1997, 386, 143-149.

[4] Liang, Q.; Li, D.; Han, H. *Materials* 2012, 5, 851-856.

[5] Ignatov, A. I.; Merzlikin, A. M.; Levy, M. Vinogradov, A. P. *Materials* 2012, 5, 1055-1083.

[6] Thapa, K. B.; Kumar, R.; Gupta, A. K. *J. Optoelectron. Adv. M.* 2010, 12, 1670-1675.

[7] Qi, L. M.; Yang, Z. Q.; Lan, F.; Gao, X.; Li, D. Z. *Chin. Phys. B* 2010, 19, 034210.

[8] Mekis, A.; Chen, J. C.; Kurland, I.; Fan, S.; Villeneuve, P. R. Joannopoulos, J. D. *Phys. Rev. Lett.* 1996, 77, 3787-3790.

[9] Naimi, . K.; Vekilov, Y. K. *Solid State Commun.* 2015, 209, 15-17.

[10] Wang, L. H.; Yang, S. H. *IEEE 2nd ISNE* 2013, 450-454.

[11] Munera, N.; Herrera, R. A. *Opt. Commun.* 2016, 368, 185-189.

[12] Karasawa, N. *Opt. Commun.* 2016, 364, 1-8.

[13] Johnson, S. G.; Mekis, A.; Fan, S.; Joannopoulos, J. D. *Computing Sci. Eng.* 2001, 3, 38-47.

[14] Shang, G. L.; Fei, G. T.; Li, D. Z. *J. Appl. D: Appl. Phys.* 2015, 48, 435304.

[15] Lourtioz, J. M.; Benisty, H.; Gerard, J. M.; Maystre, D.; Tchelnokov, A. Photonic Crystals: Towards Nanoscale Photonic Devices. Berlin: Springer press, 2008, 198-224.

[16] Gao, B.; Shi, Z.; Boyd, R. W. *Opt. express* 2015, 23, 6491-6496.

[17] Li, Z. Y.; Zhang, Z. Q. *Phys. Rev. B* 2001, 63, 125106.

[18] Purcell, E. M. *Phys. Rev.* 1946, 69, 674-681.

[19] Busch, K.; John, S. *Phys. Rev. E* 1998, 58, 3896-3908.

[20] Zhang, T.; Shao, W. W.; Li, K. Liu, X.; Xu, J. *Opt. Commun.* 2007, 281, 1286-1292.

[21] Sakoda, K. *Optical properties of photonic crystals*. London: Springer Press; 2005,151-154.

[22] Maier, S. A. *Plasmonics: Fundamentals and Applications*. London: Springer Press; 2007, 14-19.

[23] Toader, O.; John, S. *Phys. Rev. E* 2004, 70, 046605.

[24] Cheng, C.; Xu, C. *J. Appl. Phys.* 2009, 106, 033101.

[25] Sakoda, K.; Kawai, N.; Ito, T.; Chutinan, A.; Noda, S.; Mitsuyu, T.; Hirao, K. 2001, *Phys. Rev. B* 64, 045116.

[26] Raman, A.; Fan, S. *Phys. Rev. L.* 2010, 104, 087401.

[27] Kuzmiak, V.; Maradudin, A. A. *Phys. Rev. B* 1997, 55, 7427-7444.

[28] Kuzmiak, V.; Maradudin, A. A.; Pincemin, F. *Phys. Rev. B* 1994, 50, 16835-16844.

[29] Johnson, S. G.; Joannopoulos, J. D. *Opt. Express* 2001, 8, 173-190.

[30] Shi, S.; Chen, C.; Prather, D. W. *J. Opt. Soc. Am. A* 2004, 21, 1769-1775.

[31] Shen, L. F.; He, L.; Wu, L. *Acta. Phys. Sin.* 2002, 51, 1133-1138.

[32] Rahman A T M A, Vasilev K and Majewski P 2012 Designing 1D grating for extraordinary optical transmission for TM polarization. *Photonic. Nanostruct.* **10** 112-8

[33] Zong, Y. X.; Xia, J. B. *Sci. China Phys. Mech.* 2015, 58, 077201.

[34] Zong, Y. X.; Xia, J. B. *J. Appl. D: Appl. Phys.* 2015, 48, 355103.

[35] Sukhoivanov, I. A.; Guryev, I. V. *Photonic Crystals: Physics and Practical Modeling*. Berlin: Springer press, 2009, 16-20.

[36] Raether, H. *Surface plasmons on smooth and rough surfaces and on gratings.* London: Springer Press, 1988, 16-18.

[37] Ebbesen, T. W.; Lezec, H. J.; Ghaemi, H. F.; Thio, T. and Wolff, P. A. *Nature* 1998, 391, 667-669.